



Enhanced photovoltaic performance of a dye sensitized solar cell with Cu/N Co-doped TiO₂ nanoparticles

Mahesh Dhonde¹ · Kirti Sahu² · V. V. S. Murty² · Siva Sankar Nemala³ · Parag Bhargava³ · Sudhanshu Mallick³

Received: 9 September 2017 / Accepted: 14 January 2018 / Published online: 19 January 2018
© Springer Science+Business Media, LLC, part of Springer Nature 2018

Abstract

Pure and Copper/Nitrogen (Cu/N)-codoped TiO₂ photoanodes with various Cu concentrations are prepared via sol–gel route for the photoanode application in dye-sensitized solar cells (DSSCs). All the prepared samples are characterized by X-Ray Diffraction (XRD), X-Ray Photoelectron Spectroscopy (XPS), Scanning Electron Microscope (SEM), Transmission Electron Microscopy (TEM), UV–Vis spectroscopy (UV–VIS) and Electrochemical Impedance Spectroscopy (EIS). Addition of suitable amount of Cu and N content in TiO₂ can alter its optical and electrical properties by extending absorption in the visible region and band gap reduction. The results show that some of the Ti sites are replaced by Cu atoms while O sites are occupied by N atoms. Upon adequate addition of Cu/N could lead to smaller particle size, higher specific surface area, increased dye adsorption and retarded charge carrier recombination. A significant improvement in the power conversion efficiency is observed in case of optimized 0.3 mol% Cu/N-doped TiO₂ nanoparticles (NPs) based DSSC. This optimized 0.3 mol% Cu/N-doped photoanode accomplished a best power conversion efficiency of 11.70% with a short circuit current density of 23.41 mA cm⁻² which is 41% higher than that of the pure TiO₂ photoanode based DSSC (6.82%).

1 Introduction

Dye-sensitized solar cells are considered to be the most promising third generation solar cells due to their high performance, low cost, high throughput and eco-friendly manufacturing process [1, 2]. Typically a DSSC consists of a dye decorated TiO₂ photoanode, an electrolyte and a platinum coated counter electrode. The first DSSC was fabricated by M. Gratzel and team in 1991 with a power conversion efficiency of approximately 7%. Up to now, a maximum of 14.1% power conversion efficiency has been achieved which could be a potential alternatives for conventional silicon-solar cells [3]. However, DSSCs still facing challenges like stability and low power conversion efficiency unlike conventional Si-based solar cells [4]. TiO₂ is one of the most

extensively explored semiconductor-oxide material for the DSSC photoanode applications and for other photocatalysis operations such as hydrogen production, water purification and air purification due to its low cost, nontoxicity, high stability and high energy conversion efficiency. An extensive work has been reported in the literature for enhancing the performance of TiO₂ by metal doping (Ag, Au, W, Zn, Cd, Zr, Cu) [1, 2, 5–10] and nitrogen doping [1, 11–13].

Incorporation of metals in to TiO₂ structure alter its optical and electrical properties by lowering its band gap, increased visible light absorption and thereby contributing to enhanced photocurrent and reduced charge carrier recombination in DSSCs [1, 5, 14]. Similarly doping of TiO₂ with non-metals like N could contribute to lower band gap values and improved photocatalytic activity. Furthermore, presence of N conglomerates elements which lead to increased specific surface area, elevated dye loading, smooth charge carrier transfer, decreased charge carrier recombination and enhanced capacitive performance [1, 9, 15, 16]. Therefore a suitable combination of Cu and N can produce highly efficient DSSCs. Although there are very few reports have been reported in the literature with Cu/N-doped TiO₂ and other semiconductor oxide materials [17–19]. Recently Park et al. achieved 11.35% power conversion efficiency with Cu/N-doped TiO₂ NPs on an active area of 0.09 cm² [18].

✉ Mahesh Dhonde
maheshdhonde86@gmail.com

¹ Department of Physics, Prestige Institute of Engineering Management & Research, Indore, MP 452001, India

² Department of Physics, Govt. Holkar Science College, Indore, MP 452001, India

³ Department of Metallurgical Engineering & Materials Science, Indian Institute of Technology-Bombay, Mumbai, MH 40076, India

Inspired from these results, herein we report the synthesis of pure and Cu/N-doped TiO₂ NPs by modified sol–gel method and their successful incorporation in DSSCs. The combined effect of Cu and N doping on the performance of TiO₂ NPs was assessed by varying the Cu content keeping the N percentage constant. Furthermore, the photovoltaic properties of photoanodes incorporating pure and Cu/N-doped TiO₂ NPs were evaluated.

2 Experimental

2.1 Chemicals

Titanium Tetra Isopropoxide (TTIP), Titanium tetra chloride (TiCl₄) and Triton X-100 were supplied by Sigma Aldrich. Copper (II) nitrate tri hydrate [Cu(NO₃)₂·3H₂O], glacial acetic acid, ethanol, poly ethylene glycol (PEG), isopropyl alcohol (IPA) and Hydrochloric acid (HCl) were supplied by Merck. Di-tetrabutylammonium *cis*-bis(isothiocyanato) bis(2,2'-bipyridyl-4,4'-dicarboxylato) ruthenium (II) (dye N719) and 4-*tert* butylpyridine (TBP) were supplied by Solaronix. All these reagents are of analytical grade and used without any further purification.

2.2 Synthesis of pure, N and Cu/N-doped TiO₂ nanoparticles

Pure and Cu/N-doped samples were prepared by traditional sol–gel method. The precursor solution consisted of titanium tetra isopropoxide, ethanol and deionised water. A stoichiometric amount of TTIP was added to ethanol to form a precursor solution A. Another solution B was formed by the addition of Copper (II) nitrate with 0.1–0.5 mol% in 100 ml deionised water and ethanol followed by the addition of 0.5 ml glacial acetic acid. Solution B was then added drop wise into the solution A under constant magnetic stirring for 2 h to form a uniform and homogeneous solution. Hydrochloric acid was then added to each solution so as to maintain pH 4. The entire process was done under vigorous magnetic stirring at room temperature. The resultant mixture was kept for ageing at room temperature for a day and then dried in hot air oven at 80 °C. Obtained solids were ground well and calcined at 450 °C in air to obtain pure TiO₂ and Cu-doped TiO₂. To prepare N-doped TiO₂ and Cu/N-doped TiO₂ NPs subsequently second round of sintering was employed. For this pure and Cu-doped TiO₂ NPs with diverse Cu content were heated in NH₃ (33%)/N₂ atmosphere at 450 °C for 2 h in a tubular furnace at a heating rate of 5 °C min⁻¹.

2.3 Preparation of DSSC photoanodes

Pure and Cu/N-doped TiO₂ pastes were prepared as discussed in our previous work [9]. The prepared pastes were stirred well for more than 5 days to obtain a paste with desired viscosity. Fluorine-doped tin oxide (FTO) glass substrates were cut in the uniform sized substrates of 3 × 4 cm. All the substrates were cleaned well separately with water, acetone and ethanol in an ultrasonic bath for 10 min each. Then the substrates were soaked in a solution containing 40 mM TiCl₄ for 20 min at 50 °C and washed with water and ethanol to remove excess TiCl₄. After this all substrates were heat treated in the air at 450 °C for 1 h and again cleaned with water and ethanol. All cleaned 3 × 3 cm substrates were then coated with pure TiO₂ and Cu/N-doped TiO₂ pastes using doctor blade technique [9]. All the substrates were dried at 60 °C for 30 min and then kept in an electric furnace at 450 °C for 2 h at a ramp rate of 5 °C min⁻¹. The prepared substrates were again coated with TiCl₄ by dipping in a 40 mM TiCl₄ solution at 70 °C for 20 min and then kept for calcination at 450 °C for 30 min [20, 21]. After cooling to room temperature all substrates were immersed in N719 (0.3 mM) dye for 24 h for sensitizer dye loading.

2.4 Preparation of DSSC assembly

The Pt counter electrode was prepared by the deposition of Pt film with 40 nm thickness on a cleaned FTO using metal sputter with a deposition rate of 6 nm min⁻¹. Dye adsorbed photoanode and Pt counter electrode were joined together with a thin transparent Surlyn (Dupont) film of approximately 60 μm thickness. Next, an electrolyte solution containing 0.5 M of LiI, 0.05 M of I₂ and 0.5 M of 4-*tert*-butylpyridine and 0.5 M of 1-butyl-3-methylimidazolium iodide in acetonitrile was then poured into the interspace between photoanode and Pt counter electrode. Finally, the device was sealed by heating a Surlyn sheet (Dupont).

2.5 TiO₂ and photovoltaic characterization

The crystal structure of prepared pure TiO₂ and Cu/N-doped TiO₂ NPs was estimated by XRD (Expert Pro, 40 kV, 30 mA, Panalytical) with Cu Kα source. UV–Vis absorption spectra were measured by UV–Vis spectrophotometer (Perkin Elmer, Lambda25). The surface morphology and particle size of the powdered samples were analyzed by FEG-SEM (JEOL, JSM-7600F) and TEM (JEM-2010, JEOL) respectively. The specific surface areas of pure and Cu/N-doped TiO₂ NPs were measured by Brunauer, Emmett & Teller method (BET Autosorb iQ2, Quantachrome Instruments Co.). The chemical composition of

the prepared nanoparticles was confirmed by XPS measurement (ULVAC-PHI, PHI5000VersaProbell). The EIS was carried out on the Autolab measurement system for the DSSCs under AM 1.5G simulated solar illumination at 100 mW cm^{-2} , at a frequency range of 100 kHz–0.1 Hz. The applied bias voltage and ac amplitude were set at open circuit voltage (V_{oc}) at 0.1 mV. Thickness of the TiO_2 and Pt films was measured by profilometer (Dektak XT profilometer, Icon Analytical). For the DSSCs performance evaluation, a Keithley 2420 source measure unit was used to measure the J–V characteristic curve under light illumination generated by a 150 W xenon lamp on a Newport solar simulator with air mass (AM) 1.5 G filter. The incident photon-to-current conversion efficiencies (IPCE) of the DSSCs were measured by Bentham PVE300 measurement system. The active area of cell was 0.16 cm^2 .

3 Results and discussion

The XRD peaks for pure and Cu/N-doped TiO_2 with different Cu content were shown in Fig. 1. The entire XRD pattern clearly shows five main peaks of anatase phase structure of TiO_2 , namely, the planes (101), (004), (200), (105) and (211) at 2θ values of approximately 25.42, 37.91, 48.19, 54.01, and 55.19 respectively, which all are in good agreement with JCPDS card no. 21-1272. No rutile phase was observed in whole XRD pattern, which confirms that only crystalline phases were formed during synthesis process. No extra peaks for Cu/N were observed, suggesting homogeneous distribution of Cu/N with Ti in the material. Furthermore, N-doped TiO_2 NPs exhibited the anatase phase and addition of Cu didn't cause any phase change. As the N concentration was kept constant therefore addition of Cu content was a critical factor which could affect the crystal structure of TiO_2 . It was found that with the increase in Cu content peak intensities of anatase phase decreased which

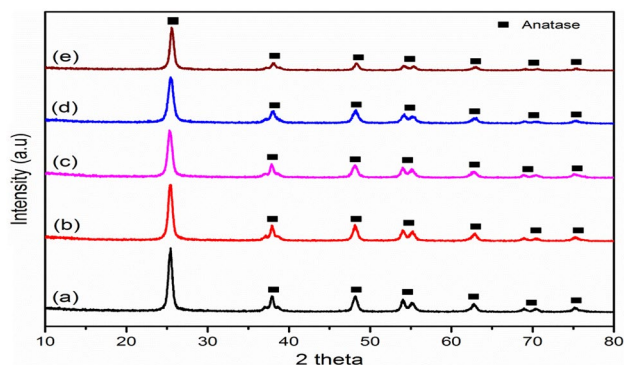


Fig. 1 XRD patterns of Pure TiO_2 NPs (a), 0.0 mol% Cu/N-doped TiO_2 NPs (b), 0.1 mol% Cu/N-doped TiO_2 NPs (c), 0.3 mol% Cu/N-doped TiO_2 NPs (d), and 0.5 mol% Cu/N-doped TiO_2 NPs (e)

indicates that the doping of Cu hinders the growth of TiO_2 nano structure [22–24].

The average crystallite size of all the samples was calculated by Scherrer's equation [25–27]. The crystallite sizes of pure and Cu/N-doped TiO_2 with Cu content 0, 0.1, 0.3, 0.5 mol% were found to be 9.86, 8.64, 7.32, 6.36 and 7.89 nm respectively. It clearly suggests that incorporation of Cu in TiO_2 matrix effectively hinders its crystal growth and stabilizes the structure.

In order to confirm the doping of Cu and N into TiO_2 nanostructure, XPS measurement was performed. Figure 2a shows the survey spectrum of optimized 0.3 mol% Cu/N-doped TiO_2 NPs. Further, the core level spectra of Cu 2p_{1/2}, Cu 2p_{3/2}, N1s, Ti 2p_{1/2} and 2p_{3/2} were shown in Fig. 2b–d respectively. The characteristic peaks of Ti 2p_{1/2} and 2p_{3/2} were observed at 464.04 and 458.29 eV respectively. Other peaks designated as N1s, Cu 2p_{1/2} and Cu 2p_{3/2} were observed at 399.18, 952.18 and 932.18 eV respectively, which were equivalent to the binding energies of N and Cu [28]. These results clearly indicate the presence of Cu and N within the TiO_2 nanostructure.

To evaluate optical responses of the prepared pure and Cu/N-doped TiO_2 NPs, UV–Vis absorption spectra were measured. Figure 3a shows the absorption spectra of the various dye adsorbed pure and Cu/N-doped photoanodes. Figure 3b shows the dye desorbed spectra of the pure and Cu/N-doped TiO_2 NPs. The absorption peaks of N-doped TiO_2 were found to be shifted towards higher wavelength side when compared to pure TiO_2 . The insertion of Cu in to TiO_2 lattice resulted further apparent shift of the spectra towards visible spectrum due to newly formed combined state. An absorption peak in the visible region was observed and this absorption increased with increasing Cu content up to a critical limit [28, 29]. Addition of Cu beyond a critical limit could lead to decreased light absorption resulting in increased band gap and decreased particle size of TiO_2 . The band gaps of pure, 0.0, 0.1, 0.3 and 0.5 mol% Cu/N-doped TiO_2 NPs are 3.15, 3.05, 2.94, 2.78, and 3.06 eV respectively. These results clearly suggest that Cu/N-doped TiO_2 NPs can respond effectively under visible light irradiation.

The FEG-SEM images of the pure, 0.3 and 0.5 mol% Cu/N-doped TiO_2 NPs were shown in Fig. 4. The optimized 0.3 mol% Cu/N-doped TiO_2 NPs had uniformly distributed spherical shaped particles. However, 0.5 mol% Cu/N-doped TiO_2 NPs had irregular, non uniform and slightly agglomerated particles. It is evident from the images that higher Cu content in TiO_2 (in case of 0.5 mol% Cu/N) could lead to agglomeration of the particles due to reduced particle size and consequently it could be a reason for reduced dye elevation and low short-circuit current of the DSSCs.

TEM images of the pure and Cu/N-doped TiO_2 NPs are shown in Fig. 5. All the synthesized pure and Cu/N-doped TiO_2 NPs were highly aggregated due to smaller particle

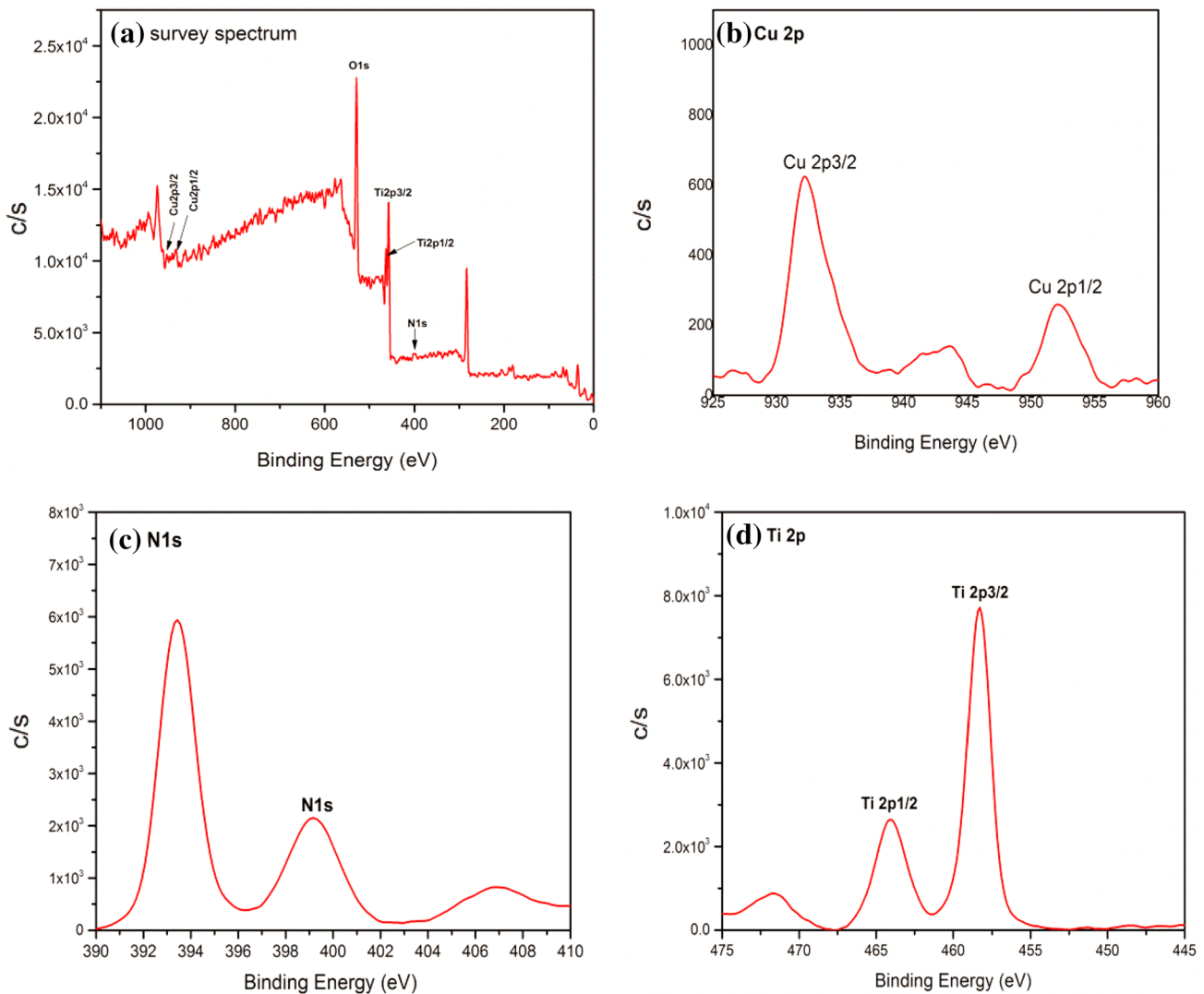


Fig. 2 XPS spectrum of optimized 0.3 mol% Cu/N-doped TiO₂ NPs: **a** survey spectrum, **b** Cu 2p peaks, **c** N1s peak and **d** Ti 2p peaks

sizes. The size of the pure TiO₂ NPs was in the range of 10–50 nm whereas N-doped TiO₂ NPs had the particle size in the range of 20–30 nm. The Cu/N-doped TiO₂ NPs with Cu concentration of 0.1, 0.3 and 0.5 mol% had particle size in the range of 10–40, 10–30 and 20–50 nm respectively.

The specific surface areas of pure and Cu/N-doped TiO₂ NPs were measured by Brunauer, Emmett & Teller method. The BET surface area of the 0.3 mol% Cu/N-doped TiO₂ NPs was 136.8 gm⁻² which was almost twice the surface area of Pure TiO₂ NPs (64.12 gm⁻²). It was found that the BET surface areas of the synthesized NPs were strongly contingent on the Cu content. The surface area of N-doped TiO₂ NPs (no Cu content) was found to be 68.26 gm⁻². An increase in surface area was observed with the increase in Cu content up to an optimal value 0.3 mol%. However when Cu content increased beyond this optimal value, surface

area decreased dramatically. The specific surface areas of 0.1 and 0.5 mol% Cu/N-doped TiO₂ NPs were 110.36 and 58.26 gm⁻² respectively.

Furthermore, using UV–Vis spectroscopy amount of dye loading in various pure and Cu/N-doped TiO₂ photoanodes were estimated using the desorbed dye from the pure and Cu/N-doped TiO₂ samples with 1 mM NaOH [30]. The adsorption spectra for the pure and Cu/N-doped samples were shown in Fig. 3b. It can be seen from the Fig. 3b that 0.3 mol% Cu/N-doped TiO₂ photoanode displays an apparent elevated dye loading compared to the other photoanodes. The N-doped TiO₂ photoanode shows a comparable dye loading to that of pure TiO₂ photoanode. A sharp increase in dye loading was observed upon introduction of Cu up to an optimum value. As the amount of Cu content increased beyond the optimum value, dye loading decreased

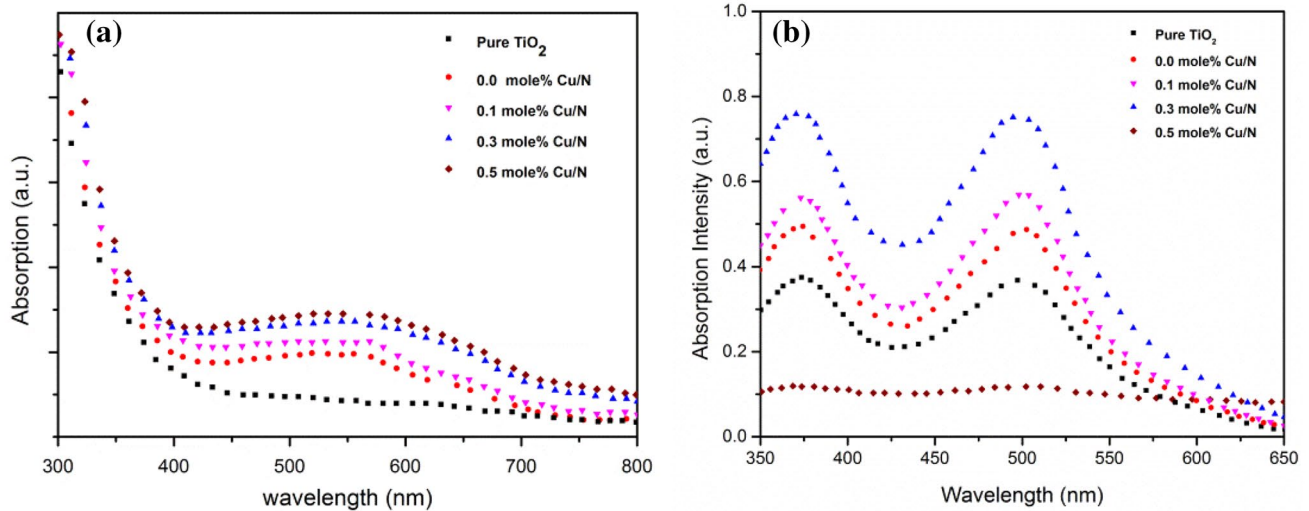


Fig. 3 UV-Vis spectra of pure TiO₂ NPs and various Cu/N-doped TiO₂ NPs (a), adsorption spectra of dye N719 desorbed photoanodes made from pure TiO₂ NPs and various Cu/N-doped TiO₂ NPs (b)

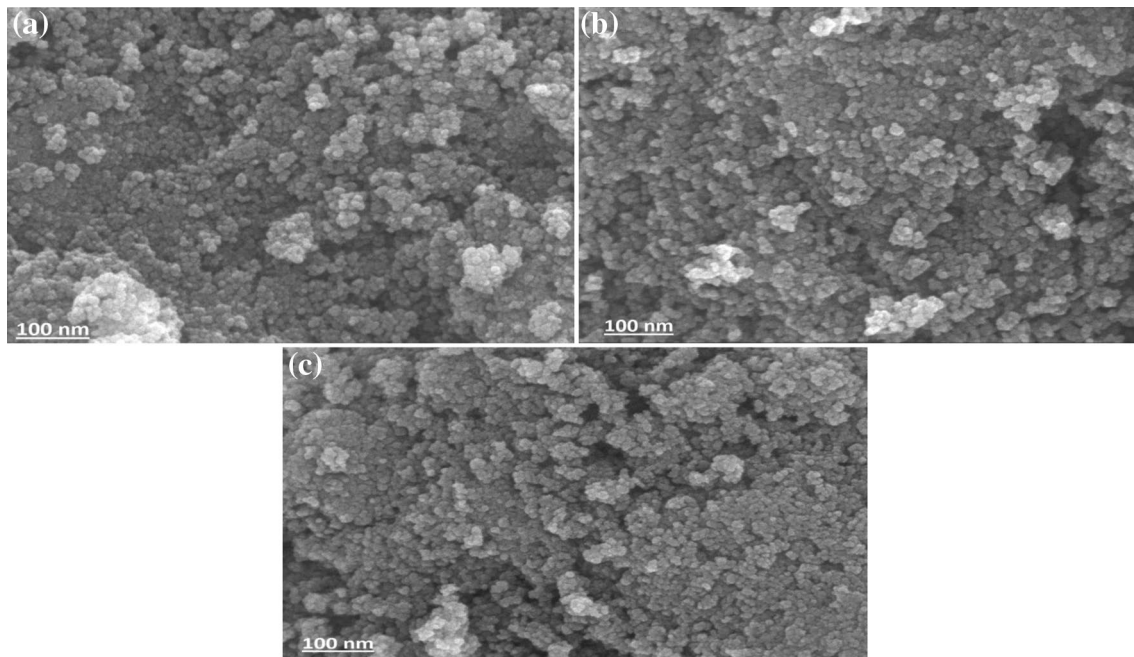


Fig. 4 FE-SEM images of the pure TiO₂ NPs (a), 0.3 mol% Cu/N-doped TiO₂ NPs (b) and 0.5 mol% Cu/N-doped TiO₂ NPs (c)

dramatically because of non uniform particle sizes, aggregation of the crystallites and reduced surface area [14, 31, 32]. The amounts of N719 dye loading on different photoanodes were shown in Table 1.

Electrochemical Impedance Spectroscopy (EIS) was performed to investigate the characteristics charge transfer properties of the DSSCs. Figure 6 shows the EIS spectra of the pure and optimized 0.3 mol% Cu/N-doped TiO₂

photoanodes measured under 1sun illumination with DC bias voltage of 0.7 V [29]. Generally EIS spectra consist of three semicircles, the first semicircle from left to right depicts the transport resistance whereas the second and third semicircle represent recombination resistance and diffusion resistance respectively. All these three semicircles attributed to resistances at the Pt counter electrode, charge transfer resistance of TiO₂/dye/electrolyte and Nernst diffusion in

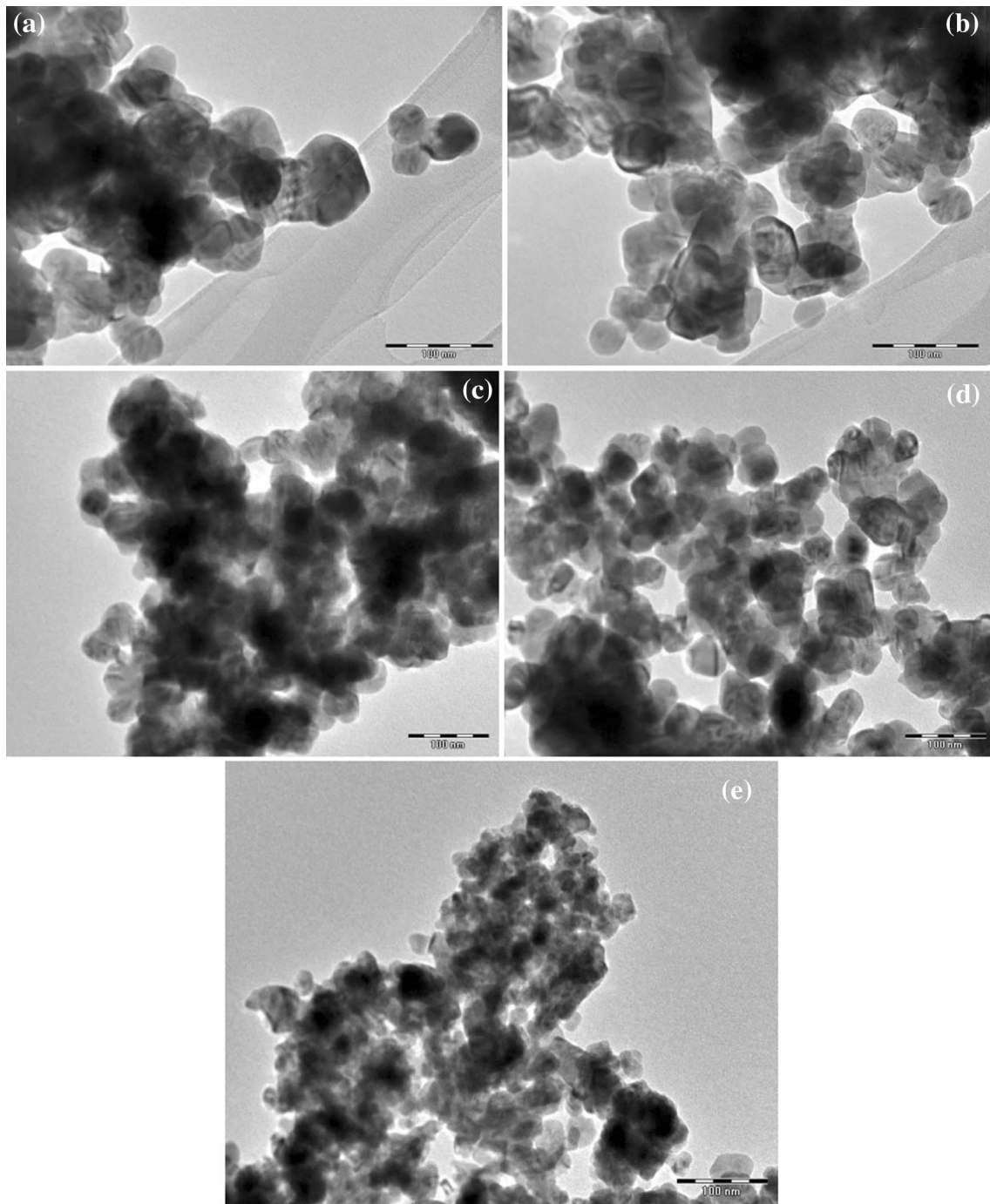


Fig. 5 TEM images of pure TiO₂ NPs (a), 0.0 mol% Cu/N TiO₂ NPs (b), 0.1 mol% Cu/N TiO₂ NPs (c), 0.3 mol% Cu/N TiO₂ NPs (d), 0.5 mol% Cu/N-doped TiO₂ NPs (e)

I⁻/I₃⁻ electrolyte [33]. In this way, the total resistance of the DSSCs is the sum of all three resistances.

It is evident from the EIS spectra that upon adequate addition of Cu/N the charge transfer and recombination resistances can be modified greatly. The diameters of the semicircles for 0.3 mol% Cu/N-doped TiO₂ photoanode were found to be smaller than that of pure TiO₂ photoanode, indicating

lower charge transfer resistance at TiO₂/dye/electrolyte interface promising enhanced electron transfer rates and reduced charge carrier recombination [34–37].

The photovoltaic performance and the efficiency of the prepared pure and Cu/N-doped TiO₂ photoanodes were measured under standard temperature condition (1 sun; input power 100 mW cm⁻²; AM 1.5) using photo current density

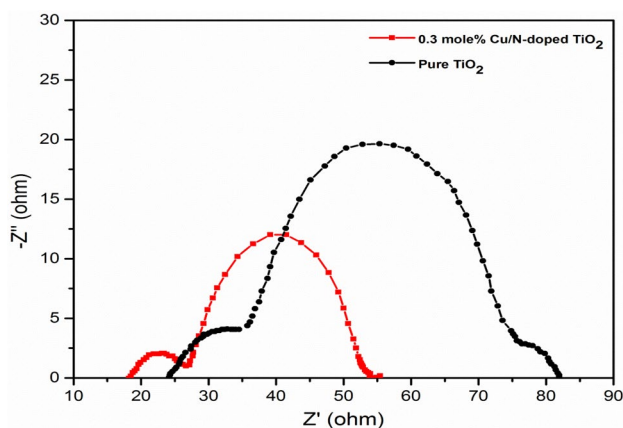


Fig. 6 EIS spectra of DSSCs based on pure and 0.3 mol% Cu/N-doped TiO₂ photoanodes

(J) as a function of the voltage as shown in Fig. 7. The corresponding photovoltaic parameters such as short circuit current density (J_{sc}), open circuit voltage (V_{oc}), maximum power point values, fill factor (FF) and power conversion efficiency (η) were calculated using solar simulator when light illumination is simulated on an active area of 0.16 cm². The obtained results were calculated and are listed in Table 1. The reported values for the photovoltaic parameters such as short circuit current density (J_{sc}), open circuit voltage (V_{oc}), fill factor (FF) and power conversion efficiency (η) are the best results among the three sample cells.

In the present work the N-doped TiO₂ photoanode displayed a power conversion efficiency of 8.42% which was 19% higher than that of synthesized pure TiO₂ NPs based photoanode. Obviously, N-doping altered the band gap of TiO₂ and extended its light absorption in the visible range. Further, addition of 0.3 mol% Cu in N-doped TiO₂ displayed a significant increase in the short circuit current density (J_{sc}),

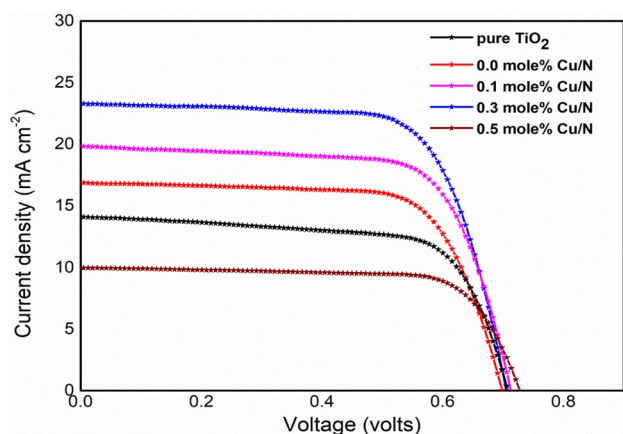


Fig. 7 J–V characteristics of DSSCs based on pure and various Cu/N-doped TiO₂ photoanodes

open circuit voltage (V_{oc}), fill factor (FF) and power conversion efficiency (η). Here, 0.3 mol% Cu/N-doped TiO₂ photoanode accomplished a power conversion efficiency of 11.70% which was 41% higher than that of pure TiO₂ NPs photoanode. This enhanced performance is attributed to appropriate particles size, increased specific surface area and reduced band gap values thereby contributing elevated dye loading, enhanced light absorption and greater short circuit current. However, higher concentration of Cu content in TiO₂ lead to decrease in available specific surface area, lower dye elevation, lower charge carrier transfer, increased recombination and hence low power conversion efficiency.

The incident photon-to-current conversion efficiency (IPCE) spectra of the DSSCs were carried out to understand the factors leading to a higher photo generated current. IPCE is defined as the ratio of charge carriers to the number of photons at a certain wavelength. The IPCE spectra of different DSSCs are plotted as a function of varying light wavelength in Fig. 8. This gives information about how the cell responds to a particular wavelength of light. All DSSCs peaks were observed at 525 nm corresponding to the N719 dye peak absorption. Cu/N-doped TiO₂ based DSSCs displayed a significant improvement in IPCE in the visible region compared to pure TiO₂ based DSSC except 0.5 mol% Cu/N-doped TiO₂ DSSC. This enhancement in IPCE is attributed to enhanced electron injection, rapid charge transfer, retarded charge carrier recombination and elevated dye loading [38]. These results are in good agreement with the J_{sc} values given in Table 1.

In general, the IPCE of a DSSC mainly depends upon light harvesting efficiency (η_{LH}), the electron injection efficiency from sensitizer dye to the conduction band edge of TiO₂ (η_{INJ}) and the collection efficiency of the injected

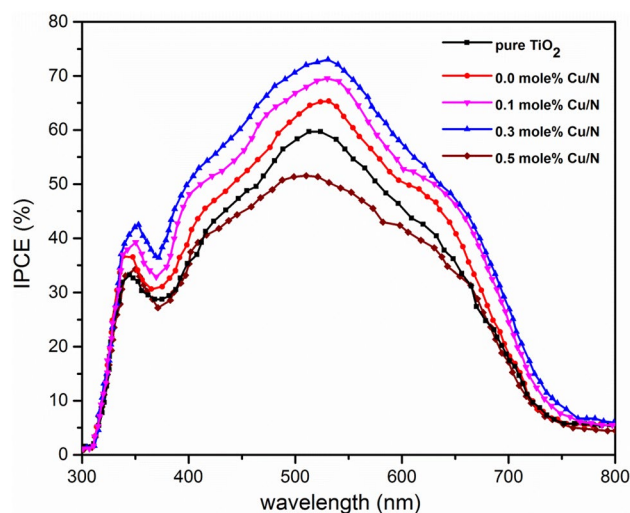


Fig. 8 IPCE spectra of pure and various Cu/N-doped TiO₂ DSSCs

Table 1 Performance parameters of the DSSCs based on pure and Cu/N-doped TiO₂ photoanodes

Sample	Jsc (mA cm ⁻²)	Voc (V)	FF (%)	η (%)	Adsorbed dye (mole cm ⁻²)
Pure TiO ₂	14.30	0.71	66.8	6.82	8.23 × 10 ⁻⁸
0.0 mol% Cu/N	17.01	0.70	65.9	8.42	9.87 × 10 ⁻⁸
0.1 mol% Cu/N	19.52	0.72	66.8	9.90	1.37 × 10 ⁻⁷
0.3 mol% Cu/N	23.41	0.71	66.8	11.70	3.24 × 10⁻⁷
0.5 mol% Cu/N	9.98	0.73	67.0	5.29	6.84 × 10 ⁻⁸

Bold parameters shows the best optimized results obtained from 0.3 mole% Cu/N-doped TiO₂ nanoparticles

Cells were tested under simulated AM 1.5 G solar illumination at 100 mW cm⁻² on an active area 0.16 cm²

electron at the back contact (η_{COLL}), which can be estimated from the given equation:

$$\text{IPCE} = \eta_{\text{LH}} \times \eta_{\text{INJ}} \times \eta_{\text{COLL}} \quad (1)$$

The light harvesting efficiency (η_{LH}) is directly relied on the amount of dye loading. In case of pure and 0.0, 0.1, 0.3 and 0.5 mol% Cu/N-doped TiO₂ the amounts of dye loading on TiO₂ photoanodes are found to be 8.23 × 10⁻⁸, 9.87 × 10⁻⁸, 1.37 × 10⁻⁷, 3.24 × 10⁻⁷ and 6.84 × 10⁻⁸ mol cm⁻² respectively. Furthermore, an efficient electron injection can take place only when the energy gap between the Lowest Unoccupied Molecular Orbital (LUMO) of the sensitizing dye and Conduction Band (CB) edge of the TiO₂ semiconductor is sufficiently high. A small decrease in energy gap between LUMO of the dye and CB of TiO₂ could decrease injection efficiency and hence IPCE of the cell [39, 40]. Moreover, the charge collection efficiency (η_{COLL}) is related to the ratio of short circuit current and total light generated current. In the present work, a significant improvement in the IPCE (approximately 73%) was observed in case of optimized 0.3 mol% Cu/N-doped TiO₂ based DSSC as compared to the pure TiO₂ based DSSC (approximately 59%).

4 Conclusions

In the present work, we synthesized pure TiO₂ and Cu/N-doped TiO₂ NPs with different Cu content by sol-gel method and successfully integrated them in DSSCs. The addition of suitable amount of Cu in TiO₂ could effectively alter its optical and electrical properties by extending absorption in the visible region and by decreasing band gap values. Furthermore, the traces of Cu/N-doped TiO₂ NPs displayed stabilized crystal structure, higher specific surface area, elevated dye loading, enhanced charge transfer and reduced charge carrier recombination. A DSSC fabricated with 0.3 mol% Cu/N-doped TiO₂ photoanode exhibited a maximum power conversion efficiency of 11.70%, which represent a dramatic improvement (about 41%) compared to power conversion efficiency of 6.82%

obtained with pure TiO₂ based DSSC. The improvement in the photovoltaic performance of the DSSCs assembled with Cu/N-doped TiO₂ NPs is attributed to the stabilized structure, higher surface area, enhanced visible light absorption, improved charge transfer and retarded charge carrier recombination.

Acknowledgements The Authors are thankful to Indian Nanoelectronics User Program (INUP) for availing financial support (project id-13DIT006) which is sponsored by DIT, MCIT, Government of India and department of Metallurgical Engineering and Materials science IITB. Authors are also thankful to V. Ganeshan, R. J. Choudhary, V. Deshpande and Mukul Gupta Scientists IUC-DAE CSR, Indore for providing guidance and lab support.

References

1. J.Y. Park, K.H. Lee, B.S. Kim, C.S. Kim, S.E. Lee, K. Okuyama, H.D. Jang, T.O. Kim, Enhancement of dye-sensitized solar cells using Zr/N-doped TiO₂ composites as photoelectrodes. *RSC Adv.* **4**, 9946 (2014)
2. Y. Lai, Z. Lin, D. Zheng, L. Chi, R. Du, C. Lin, CdSe/CdS quantum dots co-sensitized TiO₂ nanotube array photoelectrode for highly efficient solar cells dye-sensitized solar cells. *Electrochim. Acta.* **79**, 175 (2012)
3. J. Burschka, N. Pellet, S.-J. Moon, R. Humphry-Baker, P. Gao, M.K. Nazeeruddin, M. Grätzel, Sequential deposition as a route to high-performance Perovskite sensitized solar cells. *Nature* **499**, 316–319 (2013)
4. C.S. Chou, F.C. Chou, Y.G. Ding, P. Wu, The effect of ZnO-coating on the performance of a dye-sensitized solar cell. *Sol. Energy.* **86**, 1435 (2012)
5. L. Zhao, C. Zhong, Y. Wang, S. Wang, B. Dong, L. Wan, Ag nanoparticles decorated 3D flower-like TiO₂ hierarchical microstructures composed of ultrathin nanosheets and enhanced photoelectrical conversion properties in dye-sensitized solar cells. *J. Power Sources.* **292**, 49 (2015)
6. X. Zhang, F. Liu, Q.L. Huang, G. Zhou, Z.S. Wang, Dye-sensitized W-doped TiO₂ solar cells with a tunable conduction band and suppressed charge recombination. *J. Phys. Chem. C* **115**, 12665 (2011)
7. S. Muduli, O. Game, V. Dhas, K. Vijayamohan, K.A. Bogle, N. Valanoor, S.B. Ogale, TiO₂-Au plasmonic nanocomposite for enhanced dye-sensitized solar cell performance. *Sol. Energy* **86**, 1428–1434 (2012)

8. F. Huang, Q. Li, G.J. Thorogood, Y.B. Cheng, R.A. Caruso, Zn-doped TiO₂ electrodes in dye-sensitized solar cells for enhanced photocurrent. *J. Mater. Chem.* **22**, 17128–17132 (2012)
9. M. Dhonde, K. Sahu, V.V. Murty, S.S. Nemala, P. Bhargava, Surface plasmon resonance effect of Cu nanoparticles in a dye sensitized solar cell. *Electrochim. Acta.* **249**, 89–95 (2017)
10. S.M. Hosseinpour-Mashkani, M. Maddahfar, A. Sobhani-Nasab, Novel silver-doped NiTiO₃: auto-combustion synthesis, characterization and photovoltaic measurements. *S. Afr. J. Chem.* **70**, 44–48 (2017)
11. C.H. Yoon, R. Vittal, J. Lee, W.S. Chae, K.J. Kim, Enhanced performance of a dye-sensitized solar cell with an electrodeposited-platinum counter electrode. *Electrochim. Acta.* **53**, 2890 (2008)
12. H. Jiang, Q. Wang, S. Zang, J. Li, Q. Wang, Enhanced photoactivity of Sm, N, P tridoped anatase-TiO₂ nano-photocatalyst for 4-chlorophenol degradation under sunlight irradiation. *J. Haz. Mat.* **261**, 44 (2013)
13. Y.K. Lai, J.Y. Huang, H.F. Zhang, V.P. Subramaniam, Y.X. Tang, D.G. Gong, L. Sundar, L. Sun, Z. Chen, C.J. Lin, Nitrogen-doped TiO₂ nanotube array films with enhanced photocatalytic activity under various light sources., *J. Haz. Mat.* **184**, 885 (2010)
14. Y. Xie, N. Huang, S. You, Y. Liu, B. Sebo, L. Liang, X. Fang, W. Liu, S. Guo, X.Z. Zhao, Improved performance of dye-sensitized solar cells by trace amount Cr-doped TiO₂ photoelectrodes. *J. Power Sources* **224**, 168 (2013)
15. S.P. Lim, A. Pandikumar, H.N. Lim, R. Ramaraj, N.M. Huang, Boosting photovoltaic performance of dye-sensitized solar cells using silver nanoparticles decorated N,S-co-doped-TiO₂ photoanode. *Sci. Rep.* **5**, 11922 (2015)
16. H.R. Naderi, A. Sobhani-Nasab, M. Rahimi-Nasrabadi, M.R. Ganjali, Decoration of nitrogen-doped reduced graphene oxide with cobalt tungstate nanoparticles for use in high-performance supercapacitors. *Appl. Surf. Sci.* **423**:1025–1034 (2017)
17. S. Wang, X.J. Yang, Q. Jiang, J.S. Lian, Enhanced optical absorption and photocatalytic activity of Cu/N-codoped TiO₂ nanocrystals. *Mater. Sci. Semicond. Process.* **24**, 247–253 (2014)
18. J.-Y. Park, C.-S. Kim, K. Okuyama, H.-M. Lee, H.-D. Jang, S.-E. Lee, T.-O. Kim, Copper and nitrogen doping on TiO₂ photoelectrodes and their functions in dye-sensitized solar cells. *J. Power Sources* **306**, 764–771 (2016)
19. R. Gupta, N.K.R. Eswar, J.M. Modak, G. Madras, Visible light driven efficient N and Cu co-doped ZnO for photoinactivation of *Escherichia coli*. *RSC Adv.* **6**, 85675–85687 (2016)
20. C.J. Barbe, F. Arendse, P. Comte, M. Jirousek, F. Lenzenmann, V. Shklover, M. Gratzel, Nanocrystalline titanium oxide electrodes for photovoltaic applications. *J. Am. Ceram. Soc.* **80**, 3157 (1997)
21. H. Choi, C. Nahm, J. Kim, J. Moon, S. Nam, D.R. Jung, B. Park, The effect of TiCl₄-treated TiO₂ compact layer on the performance of dye-sensitized solar cell. *Curr. Appl. Phys.* **12**, 737 (2012)
22. H. Yu, B. Xue, P. Liu, J. Qiu, W. Wen, S. Zhang, H. Zhao, High-performance nanoporous TiO₂/La₂O₃ hybrid photoanode for dye-sensitized solar cells. *ACS Appl. Mater. Interfaces* **4**, 1289 (2012)
23. C.S. Kim, J.W. Shin, S.H. An, H.D. Jang, T.O. Kim, Photodegradation of volatile organic compounds using zirconium-doped TiO₂/SiO₂ visible light photocatalysts. *Chem. Eng. J.* **40**, 204–206 (2012)
24. J.A. Cha, S.H. An, H.D. Jang, C.S. Kim, D.K. Song, T.O. Kim, Synthesis and photocatalytic activity of N-doped TiO₂/ZrO₂ visible-light photocatalysts. *Adv. Powder Technol.* **23**, 717 (2011)
25. P. Cheng, C. Deng, X. Dai, B. Li, D. Liu, J. Xu, Enhanced energy conversion efficiency of TiO₂ electrode modified with WO₃ in dye-sensitized solar cells. *Photochem. Photobiol. A Chem.* **195**, 144 (2008)
26. G. Cheng, M.S. Akhtar, O.B. Yang, F.J. Stadler, Novel preparation of anatase TiO₂@reduced graphene oxide hybrids for high-performance dye-sensitized solar cells. *ACS Appl. Mater. Interfaces.* **5**, 6635 (2013)
27. J. Chae, D.Y. Kim, S. Kim, M. Kang, Photovoltaic efficiency on dye-sensitized solar cells (DSSC) assembled using Ga-incorporated TiO₂ materials. *J. Ind. Eng. Chem.* **16**, 906 (2010)
28. C.S. Kim, J.W. Shin, Y.H. Cho, H.D. Jang, H.S. Byund, T.O. Kim, Synthesis and characterization of Cu/N-doped mesoporous TiO₂ visible light photocatalysts. *Appl. Catal. A Gen.* **455**, 211 (2013)
29. Y. Jiang, Y. Yang, L. Qiang, R. Fan, H. Ning, L. Li, T. Ye, B. Yang, W. Cao, Based on Cu(II) silicotungstate modified photoanode with long electron lifetime and enhanced performance in dye sensitized solar. *J. Power Sources.* **278**, 527 (2015)
30. Y. Li, L. Jia, C. Wu, S. Han, Y. Gong, B. Chi, J. Pu, L. Jian, Mesoporous (N, S)-codoped TiO₂ nanoparticles as effective photoanode for dye-sensitized solar cells. *J. Alloys Compd.* **512**, 23 (2012)
31. C. Wang, Z. Yu, C. Bu, P. Liu, S. Bai, C. Liu, K.K. Kondamareddy W. Sun, K. Zhan, K. Zhang, S. Guo, X. Zhao, Multifunctional alumina/titania hybrid blocking layer modified nanocrystalline titania films as efficient photoanodes in dye sensitized solar cells. *J. Power Sources* **282**, 596 (2015)
32. S.H. Ko, D. Lee, H.W. Kang, K.H. Nam, J.Y. Yeo, S.J. Hong, C.P. Grigoropoulos, H.J. Sung, Nanoforest of hydrothermally grown hierarchical ZnO nanowires for a high efficiency dye-sensitized solar cell. *Nano Lett.* **11**, 666 (2011)
33. K.K. Wong, A. Ng, X.Y. Chen, Y.H. Ng, Y.H. Leung, K.H. Ho, A.B. Djurišić, A.M.C. Ng, W.K. Chan, L. Yu, D.L. Phillips, Effect of ZnO nanoparticles properties on dye sensitized solar cell performance. *ACS Appl. Mater. Interfaces* **4**, 1254–1261 (2012)
34. Y.B. Tang, C.S. Lee, J. Xu, Z.T. Liu, Z.H. Chen, Z. He, Y.L. Cao, G. Yuan, H. Song, L. Chen, L. Luo, H.M. Cheng, W.J. Zhang, I. Bello, S.T. Lee, Incorporation of graphenes in nanostructured TiO₂ films via molecular grafting for dye-sensitized solar cell application. *ACS Nano* **4**, 3482 (2010)
35. Y. Lou, S. Yuan, Y. Zhao, P. Hu, Z. Wang, M. Zhang, L. Shi, D. Li, A simple route for decorating TiO₂ nanoparticle over ZnO aggregates dye-sensitized solar cell. *Chem. Eng. J.* **229**, 190 (2013)
36. Q. Zhang, T. Gao, J.M. Andino, Y. Li, Copper and iodine co-modified TiO₂ nanoparticles for improved activity of CO₂ photoreduction with water vapor. *Appl. Catal. B Environ.* **257**, 123–124 (2012)
37. L. Tu, H. Pan, H. Xie, A. Yu, M. Xu, Q. Chai, Y. Cui, X. Zhou, Study on the fabrication and photovoltaic property of TiO₂ mesoporous microspheres. *Solid State Sci.* **14**, 616 (2012)
38. J. Qi, X. Dang, P.T. Hammond, A.M. Belcher, Highly efficient plasmon-enhanced dye-sensitized solar cells through metal@oxide core-shell nanostructure. *ACS Nano* **5**, 7108–7116 (2011)
39. A. Hagfeldt, G. Boschloo, L. Sun, L. Kloo, H. Pettersson, Dye-sensitized solar cells. *Chem. Rev.* **110**, 6595–6663 (2010)
40. K. Hara, T. Sato, R. Katoh, A. Furube, Y. Ohga, A. Shinpo, S. Suga, K. Sayama, H. Sugihara, H. Arakawa, Molecular design of coumarin dyes for efficient dye-sensitized solar cells. *J. Phys. Chem. B.* **107**, 597–606 (2003)